Control of ultranarrow Co magnetic domain wall widths in artificially patterned H-bar structures

Z. J. Yang, L. Sun, X. P. Zhang, M. Cao, X. Y. Deng, An Hu, and H. F. Ding

Control of ultranarrow Co magnetic domain wall widths in artificially patterned H-bar structures

Z. J. Yang, L. Sun, X. P. Zhang, M. Cao, X. Y. Deng, An Hu, and H. F. Ding[a)]
Department of Physics and Nanjing National Laboratory of Microstructures, Nanjing University,
22 Hankou Rd., Nanjing 210093, China

Micromagnetic simulations of Co domain walls on nanometer crossbars that join two oppositely magnetized parallel legs of "H" shaped patterns are studied. The crossbar domain walls can twist in the plane of the H-pattern, out of the plane, or swirl, forming Néel, Bloch, or vortex structures, respectively, depending on the initial configurations. An energy phase diagram as a function of the crossbar constriction yields the Néel wall as the energetically most favorable, followed by the Bloch wall, which becomes unstable and changes into a vortex-like wall with increasing crossbar size. Most interestingly, the Néel wall width can either shrink or expand depending on the crossbar dimensions. In the case that both the crossbar length and width are small, desirable, ultranarrow domain walls can be obtained. These findings are useful for spintronic device design based on domain wall pinning via nanonotch and domain-wall magnetoresistance approaches. © *2009 American Institute of Physics*. [DOI: 10.1063/1.3082046]

The rapid development of magnetic data storage is moving toward devices in the future with no moving parts, such as the proposed "race track" memory.[1] To increase storage density while avoiding the thermal instability problem (the superparamagnetic limit),[2] the challenge has become to explore the third spatial dimension. In current-driven race track memory, nanonotches have been proposed to pin domain walls[3] and the effect of the pinning has been observed.[4,5] How large a current is required to drive the domain walls and how fast the wall can be driven are key issues.[6] Recently, the threshold current was predicted to be strongly reduced when the domain wall width narrows, as the momentum transfer instead of the spin transfer effect is dominant.[7] Therefore, it is important to investigate how the domain-wall properties evolve with the nanonotech geometry. Furthermore, the reduction in the domain wall width might lead to an enhanced magnetoresistance, which is potentially useful for spintronic devices.[8,9] Domain walls also can be used as single objects in magnetic logic or memory devices.[10]

Traditionally, the width of the domain wall was believed to be determined by material parameters. However, Bruno predicted[11] and it was experimentally confirmed[12] that the Bloch domain wall width can be strongly reduced under nanometer constraints. Néel walls are commonly found in thin film systems, which are the materials of choice for spintronic devices. Thus, it is essential to understand how Néel walls evolve with geometric nanoconstraints. Micromagnetic simulations have been carried out for Néel walls in the permalloy system.[13] The wall width was reported to initially decrease with confinement and then reach a constant value without achieving ultranarrow width. The Co system was not previously addressed, but Co is appealing because its domain wall is intrinsically narrow, only ≈ 16 nm. This makes Co easier to reach the ultranarrow region under the nanoconfinement. Further, the domain-wall width of Co can be of the same order of magnitude as the confinement size, yielding a competition that may lead to interesting phenomena.

In this letter, we present micromagnetic simulations for confined Co domain walls utilizing the NIST OOMMF code.[14] As showed in Fig. 1, H-shaped samples with total length and width being $L_1 = 92$ nm and $W_1 = 300$ nm, respectively, are used. The thickness of the structures is 2 nm. The horizontal crossbar with dimensions L_0 and W_0 represents the constrained length and width, respectively. The magnetic easy axis is parallel with the two legs of the "H," as was considered by Bruno[11] for Bloch walls. Typical material parameters of Co are used: the saturation magnetization of $M_s = 1.4 \times 10^6$ A/m, the uniaxial anisotropy constant of $K_1 = 4.1 \times 10^5$ J/m^3, and the exchange constant of $A = 2.85 \times 10^{-11}$ J/m. The cell size of $1 \times 1 \times 1$ nm^3 is used in most of our simulations. To check the precision, we also compared some results with the data obtained with the cell size of $0.5 \times 0.5 \times 0.5$ nm^3 and did not find any change in our main results.

We find that different types of domain walls can be stabilized depending on the different initial configurations. We vary the initial configuration by changing the magnetization configuration of the crossbar to be parallel, perpendicular to the crossbar, or randomly distributed. Figure 2 presents three
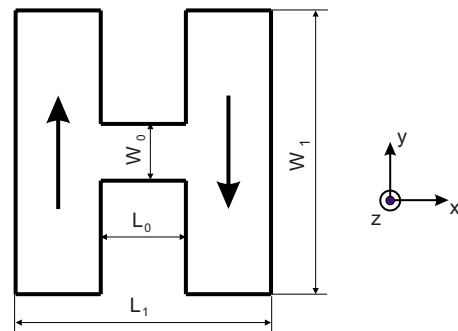

FIG. 1. (Color online) Schematic description of the H-bar geometry used in the simulation. The magnetic easy axis is along the two legs of the H, and the crossbar at the center represents the constriction. The thick arrows show the local magnetization orientation.

[a)]Author to whom correspondence should be addressed. Electronic mail: hfding@nju.edu.cn.
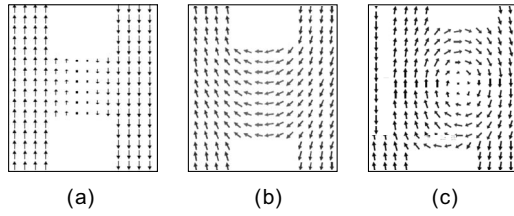
FIG. 2. Different types of domain walls obtained during the simulations. (a) Bloch wall, (b) Néel wall, and (c) vortex wall. All the images are 14 $\times$ 16 nm^2.

typical domain walls (Bloch, Néel, and vortex wall) obtained during the simulations. Typically, when the magnetization in the crossbar is configured to be perpendicular to the crossbar, a Néel wall is obtained. The other two configurations may yield the Bloch wall or vortex wall depending on the crossbar size. At a small scale of confinement (length and width), both Bloch- and Néel-type domain walls can be stabilized. With increasing dimension of the crossbar, the Bloch wall is no longer stable and changes into a vortex-type wall. The vortex wall has been experimentally observed in the permalloy system.[15]

To compare the stabilities of the different types of domain walls, we plot their total energies as the function of the crossbar size. As shown in Fig. 3, for $L_0=12$ nm, the total energies increase essentially linearly with W_0 for all three types of domain walls. The slopes are different for the different domain wall types. We can see that the total energies of the Néel wall configurations (solid squares) are considerably lower than those of the other two types of configurations for the same given geometries when $W_0 \geq 2$ nm.

It is understandable that the Néel wall is of the lowest energy for the thin film case. The total energies mainly come from the configuration confined inside the walls, and no explicit change in the magnetic configuration is found as W_0 increases. Therefore, a linear dependence with W_0 is expected. With increasing W_0, the total energy of the Bloch wall is considerably increased and the Bloch wall becomes unstable and transforms into a vortex wall. From the configuration, one can see that a vortex wall can be considered as a combination of a Bloch wall at the center and Néel walls at the outer parts. Therefore, its total energy is lower than the Bloch wall but higher than the Néel wall when W_0 is large enough for vortex formation. To check the generality of the phase diagram, we also compared the stabilities for different
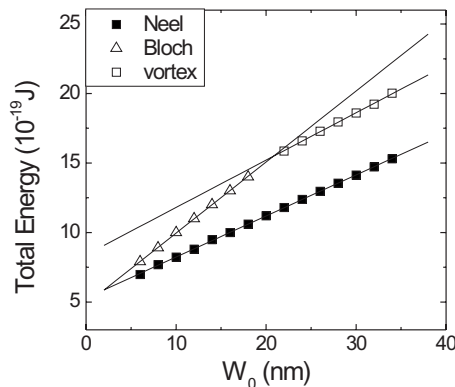

FIG. 3. Energy diagram of the different types of domain walls for L_0 simulated data and the lines are the linear fits.
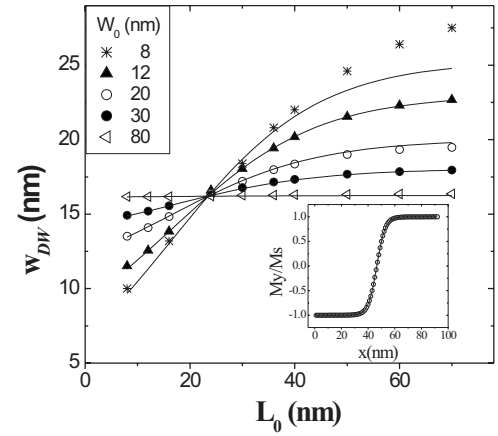

FIG. 4. Crossbar size-dependent Néel wall width. Symbols are obtained from the simulations. The lines are the fittings utilizing formula (1) shown below. The inserted figure shows the typical domain wall profile; symbols are simulated data, and the line is the fitting with the formula $M_y(x) = M_s \tanh[2(x-x_0)/W_{\mathrm{DW}}]$.

crossbar lengths L_0 (not shown), and the same conclusion can be drawn.

As presented above, the Néel wall configuration is found to be the ground state. In the following, we will focus on the crossbar size-dependent domain-wall width for the Néel walls. Quantitatively, the wall width W_{DW} is obtained via fitting the simulated position-dependent magnetization along the y direction $M_y(x)$ utilizing the formula $M_y(x) = M_s \tanh[2(x-x_0)/W_{\mathrm{DW}}]$, where M_s is the saturation magnetization and x_0 is the center position of the wall. The inset of Fig. 4 shows a typical domain-wall line profile. The symbols are the simulated data and the curve is the fitted result. As shown in the figure, in most of the cases, the function fits the simulated data well.

Figure 4 shows the Néel wall width as a function of the crossbar length L_0 for different widths W_0. Interestingly, we find that the dependence can be classified into two regions. When $L_0 < 24$ nm, the domain wall width shrinks in comparison with the standard Néel wall width without confinement W_{DW}^0. When $L_0 > 24$ nm, the domain wall expands. There is a crossover point at $L_0=24$ nm, i.e., the wall width is independent of W_0 at $L_0=24$ nm. For different W_0, the deviation in the wall width from the standard width is different. The smaller the W_0, the larger the deviation. When $W_0 > 60$ nm, the wall width is almost independent of L_0. When $W_0 < 60$ nm, the wall width shows an essential linear dependence with L_0 when $L_0 < 24$ nm. The slopes of the linear dependence depend on W_0. The slope is larger when W_0 is smaller. With further increasing L_0, the wall width deviates from a linear dependence and reaches a saturation value. The saturation values are different for different values of W_0. The smaller the value of W_0, the higher the saturation value.

To quantify the size-dependent domain wall width, we fitted the individual L_0 dependent wall width data sets for different W_0. For each set, we further identified the W_0 dependence. Interestingly, we find that most of the data can be described with a single formula shown below with $a=2.5$, $b=17.6$, $c=13.8$, and $d=13.8$ in nanometers,

$$\frac{W_{\mathrm{DW}}}{W_{\mathrm{DW}}^0} = 1 + \left[1 - \frac{a}{1 + e^{(L_0-b)/c}} \right] e^{-W_0/d}. \tag{1}$$

The fitted data are plotted as the solid lines in Fig. 4. We can find that they agree well with the simulated data (the

symbols). Only when the domain wall is strongly expanded that small deviations are found. By varying the material parameters, we find that the fitting parameter a is linearly proportional to $\sqrt{AK_1^3}/M_s$, while the other three parameters are both geometrically and material dependent.

To understand the physical picture, we initially neglect the magnetostatic energy and discuss this important effect in the next paragraph. In this case, the domain wall is determined by the competition of the exchange energy and the anisotropy energy. In the presence of the nanoconfinement, Bruno[11] pointed out that the domain wall structure can be obtained by solving the Euler equation $\ddot{\theta} + \dot{\theta}(\dot{S}/S) - [F'(\theta)/2A = 0]$, where θ, S, and $F(\theta)$ stand for the magnetization orientation, geometrical function, and the anisotropy energy, respectively. The second term, i.e., the product of the magnetization orientation gradient and the geometrical gradient divided by the geometrical function, leads to the reduction in the domain wall. When L_0 is small, the magnetization orientation gradient and the geometrical gradient appear in the same region; therefore, a reduction in the domain wall width is expected. With increasing L_0, the second term in the Euler equation decreases as the geometrical change moves toward the outside of the wall, resulting in less reduced domain wall width. Within a certain approximation, Bruno obtained a linear dependence with L_0 for the domain wall width. The reduction in the domain wall also depends on W_0. For the same given L_0, the smaller the W_0, the stronger the reduction. When the magnetostatic energy is neglected, the same argument holds for both the Bloch wall and the Néel wall cases.

In reality, the magnetostatic energy also needs to be taken into account for the estimation of the domain wall width. For the Néel wall shown in Fig. 2(b), the magnetostatic energy mainly comes from two parts, the volume charge of each side of the domain wall and the surface charge along the y direction. Both want to expand the domain wall. Similar with the exchange energy and anisotropy energy inside the confined region, the static energy caused by the volume charge is proportional to W_0. Therefore, it would not influence the domain wall width when W_0 changes. The surface charge, however, is inversely proportional to W_0. It could expand the domain wall at small W_0. When the domain wall width is very narrow, this effect, however, is mainly canceled out as the static energy can be reduced by the opposite surface charge of the same surface on each side of the domain wall. In this case, the domain wall width is mainly determined by the geometrical constriction similar as in the Bloch case. This explains our findings shown in Fig. 4 when $L_0 < 24$ nm. When the domain wall is strongly expanded,

e.g., the upper arm of $W_0 = 8$ nm, the magnetization configuration tends to deviate from the hyperbolic function used to describe the wall width. Therefore, the dependence deviates from the formula described above.

Above we discussed that the case for the magnetic easy axis is parallel to the legs of the H. When the easy axis is perpendicular to the legs, a cross wall with reduced wall width can also be found. The detailed dependence is slightly different as different types of domain walls are obtained.

In conclusion, we have investigated the nanoconfinement effect on domain walls for Co thin films via micromagnetic simulations. The Néel wall is found to be the ground state in comparison with the Bloch wall and vortex wall. The Néel wall can either shrink or expand depending on the geometric sizes. This dependence mainly comes from the competition of the nanoconfinement effect and the magnetostatic energy. In the case when both the confined width and length are small, the domain wall can reach the desirable ultranarrow limit. The findings are useful for spintronics device design based on the domain wall pinning via nanonotches and domain wall magnetoresistance approaches.

[1] S. S. P. Parkin, U.S. Patent No. 6,834,005 (21 December 2004).
[2] D. Weller and A. Moser, IEEE Trans. Magn. **35**, 4423 (1999).
[3] M. Tsoi, R. E. Fontana, and S. S. P. Parkin, Appl. Phys. Lett. **83**, 2617 (2003).
[4] M. Kläui, H. Ehrke, U. Rüiger, T. Kasama, R. E. Dunin-Borkowski, D. Backes, L. J. Heyderman, C. A. F. Vaz, J. A. C. Bland, G. Faini, E. Cambril, and W. Wernsdorfer, Appl. Phys. Lett. **87**, 102509 (2005).
[5] A. J. Zambano and J. W. P. Pratt, Appl. Phys. Lett. **85**, 1562 (2004).
[6] S. S. P. Parkin, M. Hayashi, and L. Thomas, Science **320**, 190 (2008).
[7] G. Tatara and H. Kohno, Phys. Rev. Lett. **92**, 086601 (2004).
[8] N. García, M. Muñoz, and Y.-W. Zhao, Phys. Rev. Lett. **82**, 2923 (1999).
[9] G. Tatara, Y.-W. Zhao, M. Muñoz, and N. García, Phys. Rev. Lett. **83**, 2030 (1999).
[10] D. A. Allwood, G. Xiong, M. D. Cooke, C. C. Faulkner, D. Atkinson, N. Vernier, and R. P. Cowburn, Science **296**, 2003 (2002).
[11] P. Bruno, Phys. Rev. Lett. **83**, 2425 (1999).
[12] O. Pietzsch, A. Kubetzka, M. Bode, and R. Wiesendanger, Phys. Rev. Lett. **84**, 5212 (2000).
[13] P.-O. Jubert, R. Allenspach, and A. Bichof, Phys. Rev. B **69**, 220410(R) (2004).
[14] M. J. Donahue and D. G. Porter, *OOMMF User's Guide Version 1.0* (National Institute of Standards and Technology, Gaithersburg, MD, 1999).
[15] M. Kläui, C. A. F. Vaz, J. A. C. Bland, L. J. Heyderman, F. Nolting, A. Pavlovska, E. Bauer, S. Cherifi, S. Heun, and A. Locatelli, Appl. Phys. Lett. **85**, 5637 (2004).